JOURNAL OF AIRCRAFT
Vol. 32, No. 5, September–October 1995

Effects of Strakes on a Glancing Shock Wave/Turbulent Boundary-Layer Interaction

S. Koide,* C. J. W. Griesel,† and J. L. Stollery‡
Cranfield University, Bedford MK43 0AL, England, United Kingdom

Glancing interactions, between a turbulent boundary layer and shock waves generated by an unswept sharp fin with one of five different strakes, were examined at Mach 2.46. The aim was to investigate the effects of the strakes on the interaction behavior. The experiments involved surface pressure measurements, surface oil-flow patterns and laser-light sheet pictures. An Euler computational fluid dynamics solver was used to help understand the inviscid-shock structures that play an important role in defining the interaction strength. The results show that a properly designated strake, which covers the whole of the root chord of the fin, has a weakening effect on separation. When a sharp fin is modified using a strake, the shock wave from the strake leading edge (strake shock) intersects the shock from the unmodified part of the model (fin shock) and bends it strongly towards the model. In order to prevent separation, a strake must be tall enough to prevent the fin-shock reaching the wall before the fin trailing-edge location. At the same time, the strake must be slender enough so that the strake shock itself does not cause separation. Based on these conditions, the strake dimensions needed to prevent separation have been predicted.

Nomenclature

A = area enclosed between the shock wave and the rhombic delta wing, see Fig. 5
H = height, mm
L = length, mm
M = Mach number
PR = static pressure ratio
Re = Reynolds number
X_f = distance from the unmodified-model leading edge, defined in Fig. 2
X_s, Y_s = coordinate system along and normal to the unmodified inviscid shock direction, see Fig. 2
X, Y, Z = coordinate system in directions parallel and normal to the model axis, see Fig. 2
α = half-apex (wedge) angle, deg or rad
δ = boundary-layer thickness defined by 99.5% of the external flow velocity, mm
δ^* = boundary-layer displacement thickness, mm
η = fin-shock propagation angle, see Fig. 9, deg or rad
θ = boundary-layer momentum thickness, mm
λ = strake sweep angle, see Figs. 1 and 9, deg or rad
μ = Mach angle = $\sin^{-1}(1/M)$
ξ = angle between the plane of symmetry and the face of the rhombic delta wing, see Fig. 4, deg or rad
ρ = angle of the tail of the strake, see Fig. 1, deg

Subscripts

eq = "equivalent" condition
fin = value related to the unmodified part of the model
IPS = condition to cause "incipient primary separation"
imp = value related to the fin-shock impingement point, see Fig. 9
LEF = value related to the lower edge of the fin shock, see Figs. 8 and 9
os = value related to the oblique shock wave
R = condition at the point R, see Fig. 10
req = minimum strake dimension needed to prevent separation on the wall
str = value related to the strake
∞ = freestream condition

Received Oct. 22, 1993; revision received Feb. 28, 1994; accepted for publication Feb. 28, 1995.

*Ph.D. Student, College of Aeronautics; currently at 2-4th Lab., 3rd Research Centre, Japan Defense Agency, 1-2-10 Sakae, Tachikawa, Tokyo 190, Japan. Member AIAA.
†Ph.D. Student, College of Aeronautics. Student Member AIAA.
‡Professor, Head of College of Aeronautics. Fellow AIAA.

Introduction

GLANCING interaction between a shock wave and a turbulent boundary layer can occur at many points over the body and in the intake of a high-speed flight vehicle. Once the interaction is strong enough to cause separation, several undesired phenomena may impair vehicle performance. The interaction induced by an unswept sharp fin is one of the most basic glancing interactions and it is the configuration with which this study begins. The broad features of the interaction have been summarized by Settles and Dolling.[1]

Fillets and strakes have been used extensively to modify the airflow over aircraft at subsonic speeds. Although they might also be considered attractive for decreasing the glancing interaction strength at supersonic and hypersonic speeds, available data are limited. Lakshmanan and Tiwari[2] investigated the effect of a circular fillet on the flowfield around a blunt fin/flat plate junction numerically at $M_\infty = 2.4$ and $Re = 2.6 \times 10^6$/m. They found that a fillet with a radius of 3.5 times the fin leading-edge diameter was required in order to weaken the horseshoe vortex formed in the interaction region, but their conclusion lacked experimental validation. On the other hand, a triangular-ramp-type fillet for an unswept and a swept blunt fin, examined by Blank[3] at $M_\infty = 2.45$ and $Re = 2.6 \times 10^6$/m, enlarged the size of the separated flow region rather than diminishing it. However, the strake-type modifications that Blank tried did reduce the pressure levels and shock fluctuations around the strake. Kleifges and Dolling[4] tested a similar strake for a blunt fin (at a higher Mach number) and reached a similar conclusion.

In parallel to the studies for the blunt fin, the effects of a circular fillet and three distinct strakes on an unswept sharp-fin junction were investigated[5] as a preliminary test for the

current study. Unfortunately, the fillet strengthened the interaction rather than weakened it because the inviscid shock wave, which plays an important role in specifying the interaction strength, was enhanced by the fillet. Hence, in this article, a series of modified fins are examined with emphasis on the effects of the strakes. The objectives of the study are, to understand the structure of the modified flowfields, to investigate the effects of the strake dimensions on the interaction behavior, and finally to predict the strake dimensions needed to prevent separation.

Experimental Procedures

Wind-Tunnel and Test Conditions

The experiments were conducted in Cranfield's 23 × 23 cm continuous supersonic wind tunnel at $M_\infty = 2.46 \pm 1.1\%$ and $Re = 2.59 \times 10^6/\text{m} \pm 4.4\%$ under approximately adiabatic wall temperature conditions. The tunnel stagnation pressure and stagnation temperature were 2.48×10^4 Pa ± 1.6% and 290 K ± 1.3%, respectively.

The properties of the tunnel sidewall boundary layer were thoroughly investigated by Kubota and Stollery[6] at three spanwise stations. The survey showed that the boundary layer was fully turbulent with very little spanwise variation. The boundary-layer thickness δ defined by a point where 99.5% of the external flow velocity was reached was 15.7 mm, and the corresponding displacement and momentum thicknesses δ^* and θ were 3.8 and 1.0 mm, respectively. The velocity profile was close to a 1/7th power law.

Models

Figure 1 shows the configurations of the six models employed. Each model was designed asymmetrically in order to obtain the largest model size without choking the tunnel. For convenience, the unmodified part of the model will be termed "fin" and all the variables related to this part are expressed using the suffix fin. On the other hand, all the variables related to the strake are identified by the suffix "str."

To provide "standard" data for sharp-fin induced interaction, a fin with a 15-deg half-wedge angle α_{fin} was employed as the unmodified model. The angle was chosen to create a fully separated interaction flowfield based on the observations

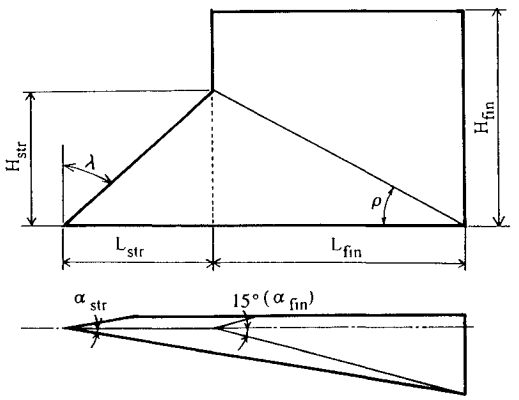

MODEL	L_{str}	H_{str}	α_{str}	λ	L_{fin}	H_{fin}
Unmodified	—	—	—	—	139.7	101.6
Strake 1	31.5	66.0	12.3°	25.5°	139.7	101.6
Strake 2	47.2	66.0	11.3°	35.6°	139.7	101.6
Strake 3	82.7	74.8	9.6°	47.9°	139.7	119.4
Strake 4	82.7	39.4	9.6°	64.5°	139.7	119.4
Strake 5	85.7	80.0	8.7°	47.0°	114.3	152.4

UNIT : mm

Fig. 1 Test models.

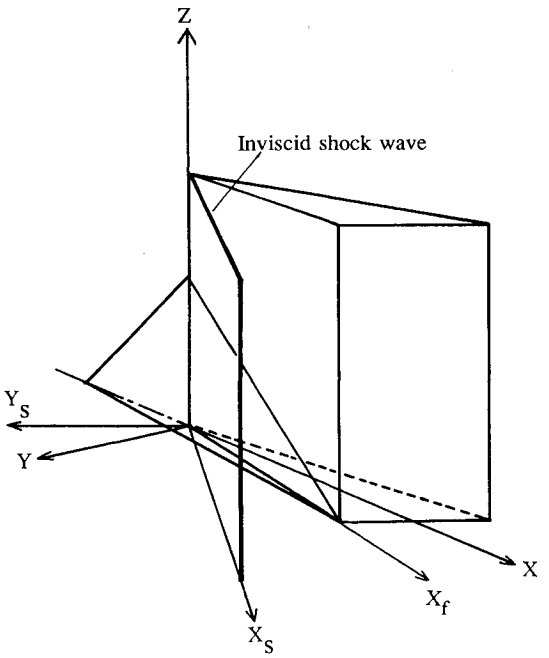

Fig. 2 Coordinate systems.

from previous investigations. The height of strakes 1 and 2 was selected to make the angle ρ (see Fig. 1) more than the Mach angle at $M_\infty = 2.46$. This angle was originally expected to prevent the shock wave, caused by the unmodified part of the model leading edge, from affecting the flow on the wall until downstream of the trailing edge. But weak separation was still observed in the cases of strakes 1 and 2 (see the following discussion). Hence, another series of strakes (strakes 3–5), whose heights and (or) lengths were larger than the first two strakes, were employed. In order to maintain a certain length of the unmodified part of the model leading edge, the latter group has an increased height H_{fin}. Strake 5 has the greatest height and length, but in order to keep the complete model within the allowable blockage ratio the fin chord L_{fin} was reduced by 25.4 mm.

Experimental Techniques

Detailed surveys of the surface pressures in the interaction region were made from readings taken at the 225 pressure tappings arranged on the tunnel wall. The accuracy of the measured static pressure was estimated to be ±3.5%. To visualize the streak patterns on the wall, the oil-flow technique (a mixture of titanium dioxide with motor oil and several drops of oleic acid) was employed. Three-dimensional flowfield surveys were made using the laser-light-sheet flow visualization (LFV) technique. Details of this technique are given in Ref. 7.

Coordinate Systems

In order to present the results, two different types of coordinate systems are employed (Fig. 2). The X, Y, and Z axes are defined in directions parallel and normal to the model axis. The X_s and Y_s axes are along and perpendicular to the unmodified inviscid shock-wave direction calculated by the oblique shock relations. In addition, a length X_f is also employed to specify a distance from the fin leading edge along the fin-wall junction as shown in Fig. 2.

Experimental Results

LFV surveys were carried out at several $Y_s - Z$ slices at different X_s locations for the unmodified fin, and for strakes 1 and 2. In Fig. 3, typical flowfield images obtained by the LFV technique are presented, together with isobars on the

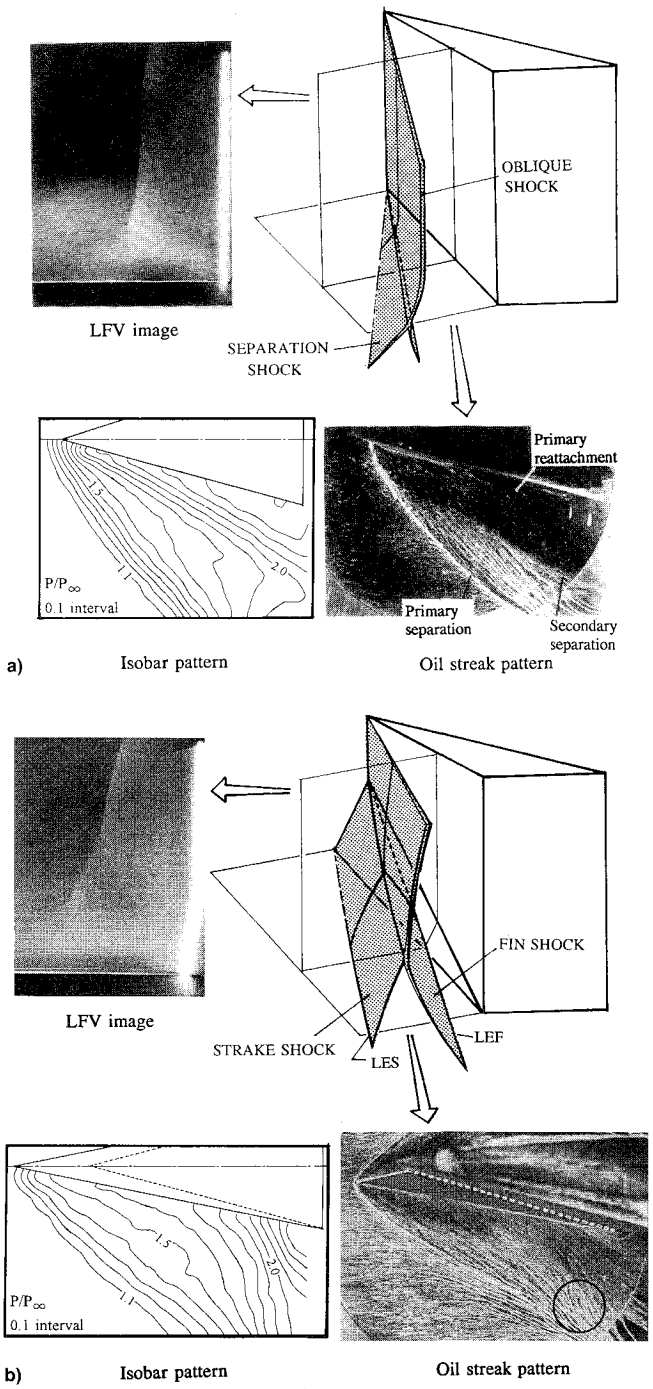

Fig. 3 Shock structure with LFV image, oil streak pattern, and isobar pattern: a) unmodified and b) strake 2.

wall, surface oil-streak patterns, and three-dimensional shock structures deduced from the LFV surveys.

The unmodified fin created a clear λ-shock structure resulting from the intersection of the separation shock and the oblique shock (see Fig. 3a). Beneath the λ foot, the core of the separation zone appears as a dark area in the LFV image. The corresponding oil-streak pattern has primary separation and reattachment lines as well as an oil convergence relating to secondary separation. In the isobar pattern, separation is recognized as a plateau region where isobars are located with wider intervals.

In the case of strake 2 (Fig. 3b), the shock from the strake leading edge (strake shock) intersects the shock from the unmodified part of the model leading edge (fin shock), and bends it strongly towards the model. It is very hard to see any λ-shock structure at the lower-edge positions of the strake- and fin-shocks, labeled LES and LEF, respectively, in Fig. 3b. Neither can a clear core of any separation zone be distinguished in the LFV image. In the oil-streak pattern, the primary separation line still exists and this indicates that some separation has occurred. However, this line becomes more diffuse and there is no sign of secondary separation. Neither can a plateau region be distinguished in the isobar pattern. It is obvious that strake 2 has had a marked effect on the interaction and has weakened separation. Strake 1 had similar qualitative flow features (not shown) to those of strake 2. However, the oil convergence into the primary separation line was more distinct, compared with strake 2,[5,7] and so this suggests that the shorter strake (strake 1) created a slightly stronger separation than that of strake 2. Based on these observations, it is reasonable to conclude that a properly designated strake, which covers the whole of the root chord, has a weakening effect on separation.

Prediction of the Strake Dimensions Needed to Prevent Separation

From the relationship between the modified shock system and the oil-flow pattern observed in Fig. 3b, the primary separation line is considered to be created by the strake shock. In addition, a sudden deflection of the oil streaks is noticed in the area marked by a circle (see the oil flow in Fig. 3b). This deflection is caused by the fin-shock impingement on the wall. The height of strake 2 prevented the fin shock from reaching the wall until near the trailing edge, however the trailing-edge area was still affected by the fin shock. Hence, a slightly taller strake might prevent the fin-shock effect completely.

If the height of the strake is tall enough to prevent the fin-shock effect, the flowfield is controlled by the strake shock instead of the fin shock. In that case, the strength of separation solely depends on the strength of the strake shock. Comparing strakes 1 and 2, the longer strake (strake 2) generated a weaker shock because of its relatively smaller apex angle α_{str} and larger sweep angle λ. Hence, the beneficial effect of strake 2 on separation was greater than the effect of strake 1. If the strake shock could be further weakened while maintaining the strake height to prevent the fin-shock effect, separation would be suppressed completely on the wall.

These observations suggest that in order to prevent separation on the wall a strake must have a geometry that 1) is long enough to weaken the strake shock and 2) is tall enough to prevent the fin shock from reaching the wall until downstream of the model trailing edge.

Based on conditions 1) and 2), the necessary geometrical requirements for a strake in terms of L_{req} and H_{req} (minimum length and height of the strakes required to prevent separation) were predicted. Note that the prediction discussed here assumes that the expansion fan from the model trailing edge "quenches" further interaction.

Estimations of the Strake-Shock Strength

In order to consider condition 1, the strength of the strake shock must be predicted for arbitrary strake dimensions and Mach numbers. To evaluate the strength, flowfields around a series of rhombic delta wings (RDWs) were calculated by an Euler computational fluid dynamics (CFD) solver developed by Griesel.[8] The RDWs generate inviscid shock waves appropriate to the strake shocks as shown in Fig. 4. Hence, the suffix str is also used for the RDW for convenience.

The CFD calculations were carried out for $30 \leq \lambda \leq 60$ deg and $8 \leq \alpha_{str} \leq 17$ deg ($\leq$14 deg at $M_\infty = 2.0$) at $M_\infty =$ 2.0, 2.46, and 3.5. This range was chosen to include the present experimental condition, together with a wider band of supersonic Mach numbers under which the shock wave remains attached to the delta-wing apex. The strength of the

strake shock was evaluated from the computed static pressure distributions in the plane of symmetry of the RDWs (see Fig. 4). This was because the local pressure rise (induced by the inviscid shock wave) in the vicinity of the wall boundary layer was considered to be of primary importance in specifying the interaction behavior. Figure 5 shows an example of the computed static pressure field in the plane of symmetry. In the case of the RDW, the pressure behind the shock wave increases gradually as the wing surface is approached because of the conical nature of the flow. To specify the pressure level by a single pressure ratio, the computed local pressure ratios in the area marked A in Fig. 5 were first integrated and the integrated value was then averaged (divided) by the area A. This averaged pressure ratio was termed "equivalent pressure ratio (PR_{eq})." In the following discussion, the term "strake-shock strength" is employed to refer to PR_{eq}, but PR_{eq} is not equal to the pressure jump across the shock in most of the cases. The solid circles in Fig. 6 show the computed values of PR_{eq} obtained at various α_{str}, λ at $M_\infty = 2.46$ (the cases at $M_\infty = 2.0$ and 3.5 are not shown here, see Ref. 7). The value at $\lambda = 0$ deg (corresponding to the value of the two-dimensional oblique shock) is also marked by a single-chain-dotted line as a reference.

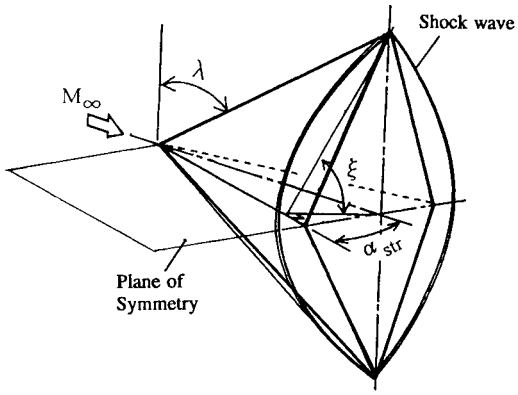

Fig. 4 Schematic view of a rhombic delta wing and its inviscid shock wave.

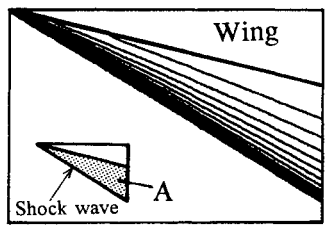

Fig. 5 Computed pressure field in the plane of symmetry of the RDW ($M_\infty = 2.46$, $\alpha_{str} = 14$ deg, $\lambda = 45$ deg).

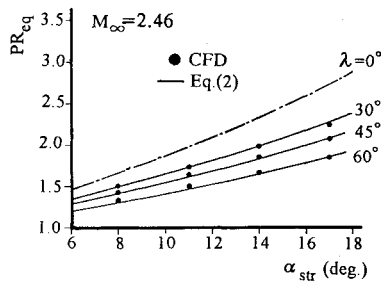

Fig. 6 Comparison of the equivalent pressure ratios by the CFD procedures and Eq. (2).

In order to predict the strake-shock strength for arbitrary α_{str}, λ, and M_∞, PR_{eq} must be correlated with them. To construct the correlation law, the angle between the plane of symmetry and the face of the delta wing

$$\xi = \tan^{-1} \frac{1}{\sin \alpha_{str} \tan \lambda} \tag{1}$$

(see Fig. 4) was introduced. When α_{str} and λ increase, ξ tends to depart from 90 deg. Similarly, PR_{eq} will decrease from its value at $\lambda = 0$ deg (i.e., the oblique shock pressure ratio for an unswept sharp fin of half-wedge angle α_{str}, expressed by PR_{os}, see the case of $\lambda = 0$ deg in Fig. 6) as ξ drops below 90 deg. Hence, a simple correlation between ξ and PR_{eq}/PR_{os} was first examined, but this did not sufficiently collapse the data obtained at different M_∞.[7] In order to improve the correlation, the data must be plotted by introducing a role for M_∞ while considering the condition that PR_{eq}/PR_{os} has to approach 1.0 when ξ approaches 90 deg. The parameter

$$\frac{PR_{eq}}{PR_{os}} \frac{2\xi}{\pi} + 0.05|M_\infty - 2.5| \left(\frac{\pi}{2} - \xi\right)$$

was finally obtained, where ξ is expressed in radians. This plot greatly improved the data correlation with ξ (see Fig. 7). Thus, the value of PR_{eq} is determined directly from

$$PR_{eq} = \frac{\pi PR_{os}\{F(\xi) - 0.05|M_\infty - 2.5|[(\pi/2) - \xi]\}}{2\xi} \tag{2}$$

where $F(\xi)$ was obtained by the least-squares method as

$$F(\xi) = -0.8808 + 2.0571\xi - 0.6355\xi^2 - 0.4630\xi^3 + 0.3277\xi^4 \tag{3}$$

The values of PR_{eq} from the CFD calculations and Eq. (2) were compared at various M_∞, α_{str}, and λ. The agreement was very good (see the example at $M_\infty = 2.46$ in Fig. 6).

Some extreme cases were calculated in order to estimate the effective range of Eq. (2) (see the cases marked by a solid circle, a solid triangle, a solid box, and a cross in Fig. 7). Based on these data, Eq. (2) has been estimated to be quite accurate (within 5% of the corresponding CFD value) for the range $2.0 \leq M_\infty \leq 5.0$, $0 \leq \alpha_{str} \leq 20$ deg, and $0 \leq \lambda \leq 70$ deg. In terms of Eq. (2), PR_{eq} can be easily specified for arbitrary α_{str}, λ, and M_∞ within the effective range of Eq. (2).

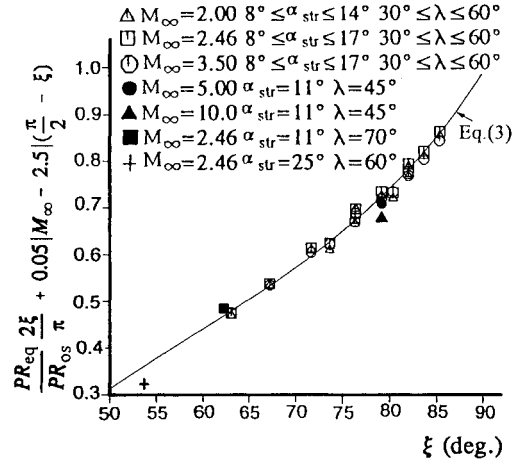

Fig. 7 Correlation of the equivalent pressure ratios.

Strake Height Required to Prevent the Fin-Shock Effect

In order to consider condition 2, the propagation angle of the LEF must be estimated. To evaluate the angle, flowfields around the fin with strakes 1–5 were calculated by the Euler CFD solver applied to the rhombic delta wings. The Euler solver does not handle viscous effects, so that it is natural that the computed inviscid flowfield tends to diverge from the actual field when the viscous effects become dominant. From comparison with the experimental LFV images, the location and the shape of the fin shock, including the part behind the strake shock, were found to be predicted quite well.[7] This is because the fin shock was not affected by the viscous force until it reached the wall boundary layer. Hence, the CFD data have been employed to investigate the propagation angle of the LEF.

Figure 8 presents the computed static pressure contours at several $Y - Z$ slices for strake 2. The contour patterns on the model surface and on the wall are also shown. In the figure, a brighter tone indicates a higher pressure level. The inviscid flow structure shown in Fig. 8 is basically the same as that deduced from the LFV images. Note that the computed fin shock attaches to the model surface while one cannot observe the fin-shock attachment in the LFV images because of the strong laser reflection from the model surface (see the example in Fig. 3b). As to the computed fin shock, the term LEF will be used to describe the part of the fin shock closest to the wall (see Fig. 8).

From the computed flow structures, it is observed that the LEF approaches the wall quite linearly with the distance from the fin leading edge (see, e.g., the contours on the model in Fig. 8) and the fin shock first impinges on the wall at a point along the strake-wall junction (see the point A in Fig. 8). Hence, the propagation angle of the LEF η could be specified easily for each model. The exact definition of η employed here is explained in Fig. 9, where the position of LEF is projected onto the $X_f - Z$ surface (the side face of the unmodified part of the model) in order to specify the angle η.

If the strake shock is treated as a two-dimensional oblique shock and PR_{eq} is introduced as the pressure rise across the shock, the Mach number behind the strake shock can be calculated from the oblique shock theory, i.e.,

$$M_{eq} = \sqrt{\frac{M_\infty^2(6PR_{eq} + 1) - 5(PR_{eq}^2 - 1)}{PR_{eq}(PR_{eq} + 6)}} \qquad (4)$$

Actually, M_{eq} is very close to the averaged Mach number behind the strake shock. The Mach angles based on M_{eq} could then be calculated from $\mu_{eq} = \sin^{-1}(1/M_{eq})$ and were compared with the propagation angles measured from the CFD

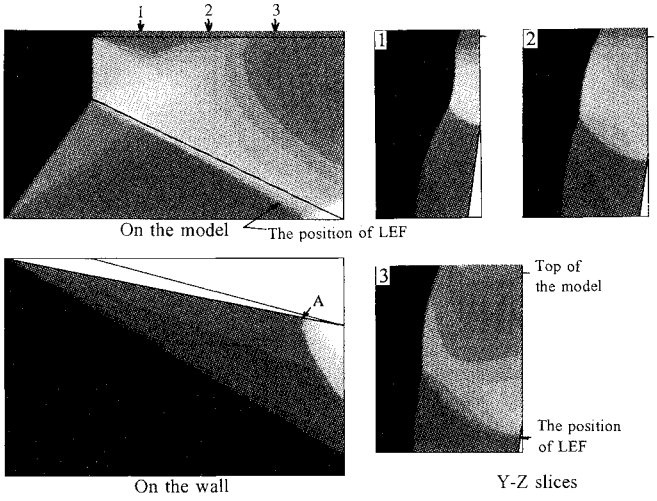

Fig. 8 Computed inviscid flowfield (strake 2, $M_\infty = 2.46$).

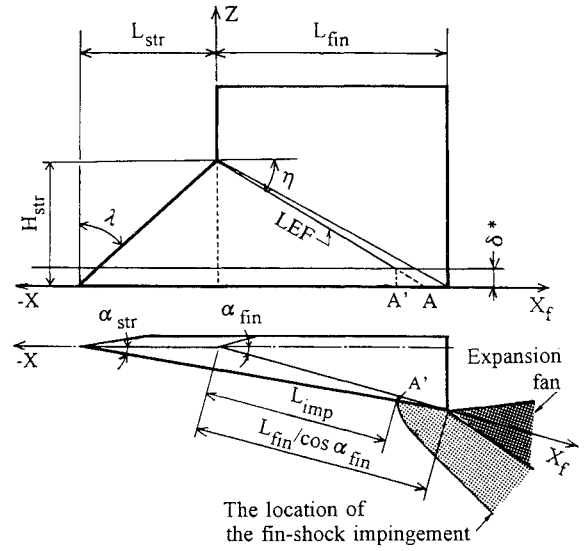

Fig. 9 Geometrical relationship among the model, the fin shock, and δ^*.

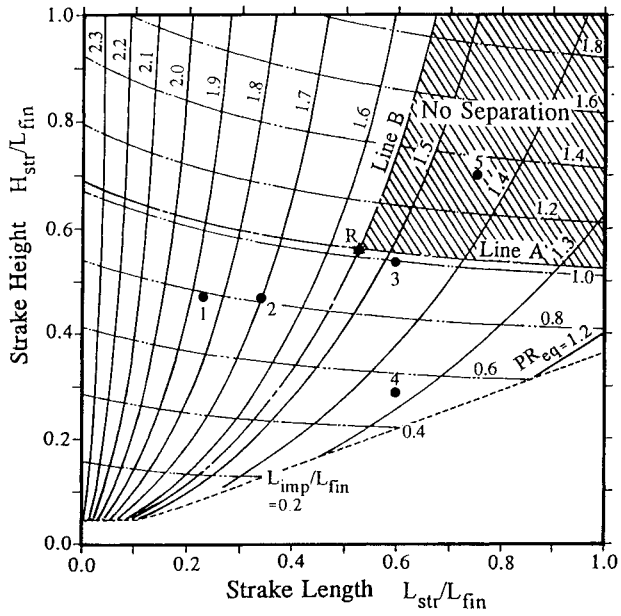

Fig. 10 Necessary strake dimensions with L_{imp}/L_{fin} and PR_{eq} ($M_\infty = 2.46$, $\alpha_{fin} = 15$ deg, $\delta^*/L_{fin} = 0.0273$).

results. The difference between the two values was quite small at all the cases examined. Hence, the Mach angle based on M_{eq} was introduced to predict the values of η:

$$\eta = \sin^{-1}(1/M_{eq}) \qquad (5)$$

From the displacement thickness concept, it is reasonable to consider that flowfield's boundary can be shifted outward by an amount equivalent to δ^* from the real wall. Hence, the fin-shock impingement point is assumed to be the intersection of the LEF and δ^*. The fin-shock impingement length L_{imp} is then determined by means of the value of η from Eq. (5) and the geometrical relation illustrated in Fig. 9 as

$$\frac{L_{imp}}{L_{fin}} = \frac{1}{\tan\eta}\left(\frac{H_{str}}{L_{fin}} - \frac{\delta^*}{L_{fin}}\right) \qquad (6)$$

The values of L_{imp}/L_{fin} are then calculated for the present experimental condition of $M_\infty = 2.46$, $\alpha_{fin} = 15$ deg and

$\delta^*/L_{fin} = 0.0273$ and are presented against L_{str}/L_{fin} and H_{str}/L_{fin} using a group of iso-L_{imp}/L_{fin} lines (see the double-chain-dotted lines in Fig. 10). The zone where the strake sweep angle λ exceeds 70 deg is not shown in Fig. 10 because this zone is beyond the effective range of Eq. (2) on which L_{imp} depends. The area of $H_{str}/L_{fin} \leq \delta^*/L_{fin}$ is also omitted because a negative value of L_{imp}/L_{fin} is meaningless. The dimensions of all the strakes tested are marked by their numbers on Fig. 10 in order to identify the level of L_{imp} for each strake.

The fin shock first reaches δ^* above the point labeled A' in Fig. 9 (note that the point A' is slightly different from point A in Fig. 8 because of δ^*). Once L_{imp} is longer than $L_{fin}/\cos\alpha_{fin}$, the expansion fan from the model trailing edge weakens the impinged fin shock and "quenches" further interaction (see Fig. 9). Hence,

$$L_{imp}/L_{fin} = 1/\cos\alpha_{fin} \tag{7}$$

can be treated as a criterion for the required strake height. The value of $L_{imp}/L_{fin} = 1.035$ at $\alpha_{fin} = 15$ deg is marked by the single-chain-dotted line labeled "Line A" in Fig. 10. A strake must have dimensions above this line in order to prevent the fin-shock effect.

Necessary Strake Dimensions Under the Present Experimental Condition

From the geometrical relation illustrated in Fig. 9, α_{str} and λ can be expressed as

$$\alpha_{str} = \tan^{-1}\frac{L_{fin}\tan\alpha_{fin}}{L_{str} + L_{fin}} = \tan^{-1}\frac{\tan\alpha_{fin}}{L_{str}/L_{fin} + 1} \tag{8}$$

$$\lambda = 90 \text{ deg} - \tan^{-1}(H_{str}/L_{str}) \tag{9}$$

By means of Eqs. (1), (2), (8), and (9), the values of PR_{eq} are obtained over a wide range of L_{str}/L_{fin} and H_{str}/L_{fin} for the present experimental case of $M_\infty = 2.46$ and $\alpha_{fin} = 15$ deg. They are presented as a group of iso-PR_{eq} lines (see the solid lines in Fig. 10).

"Line B" in Fig. 10 corresponds to the pressure level for incipient primary separation (IPS) due to an unswept sharp fin. This value of $PR_{IPS} = 1.55$ is obtained implicitly from Korkegi's criterion[9] of $M_\infty\alpha_{IPS} = 17$ deg with $M_\infty = 2.46$. Below this pressure level, the shock is not considered to be strong enough to cause separation. Hence, in order to prevent separation, a strake must have dimensions appropriate to the zone to the right of line B and above line A. This zone is hatched in Fig. 10 with the label of "no separation." The minimum required length and height of the strake (expressed by L_{req} and H_{req}) can be read from the intersection point of the lines A and B (labeled R), and they are $0.53L_{fin}$ and $0.57L_{fin}$, respectively.

As the values of L_{req}/L_{fin} and H_{req}/L_{fin} are read from the intersection of lines A and B (i.e., point R), they can be found mathematically. As mentioned above, line A is expressed by Eqs. (6) and (7). Furthermore, the level of PR_{eq} is constant at the point of R and equal to PR_{IPS}. Hence, the fin-shock propagation angle at R, η_R, can be fixed by Eqs. (4) and (5) in terms of PR_{IPS}. Substituting Eq. (7) and η_R into Eq. (6) yields

$$\frac{H_{req}}{L_{fin}} = \frac{\tan\eta_R}{\cos\alpha_{fin}} + \frac{\delta^*}{L_{fin}} \tag{10}$$

In order to specify the value of L_{req}/L_{fin}, line B is formulated by Eq. (2) as

$$\frac{\pi PR_{os}\{F(\xi) - 0.05|M_\infty - 2.5|[(\pi/2) - \xi]\}}{2\xi} = PR_{IPS} \tag{11}$$

Once the value of H_{req}/L_{fin} is fixed by Eq. (10), L_{req}/L_{fin} is then obtained by Eq. (11) implicitly. In terms of Eqs. (10) and (11), the effects of M_∞, α_{fin}, and δ^*/L_{fin} on L_{req}/L_{fin} and H_{req}/L_{fin} can be considered quantitatively and will be discussed later.

Plausibility of the Prediction

In order to consider the plausibility of the prediction, the surface oil-flow patterns for strakes 1–5 were examined (see Fig. 11). The cases of strakes 2 and 3 are not shown here (see Fig. 3b and Ref. 7). The corresponding values of PR_{eq} and L_{imp}/L_{fin} read from Fig. 10 are printed on Fig. 11. The locations of the strake shock and the fin-shock impingement, obtained by the CFD calculations, are also marked by the solid lines.

When the strake-shock strength is above the level of line B (i.e., $PR_{eq} \geq 1.55$), the oil convergence line caused by the strake shock (labeled C_1) is still clear and the primary separation observed in the unmodified case (see Fig. 3a) still survives (strakes 1 and 2 belong to this situation, see the case of strake 1 in Fig. 11a). But the convergence line is weakened and approaches the inviscid strake-shock location with reduction of PR_{eq}. Once PR_{eq} becomes less than the level of line B (corresponding to the cases of strakes 3–5), the oil coalescence C_1 becomes diffuse and disappears for the case of the weakest strake shock (strake 4, see Fig. 11b). It should be noted that the clear oil convergence C_1 whose local deflection angle exceeded the inviscid strake-shock angle was

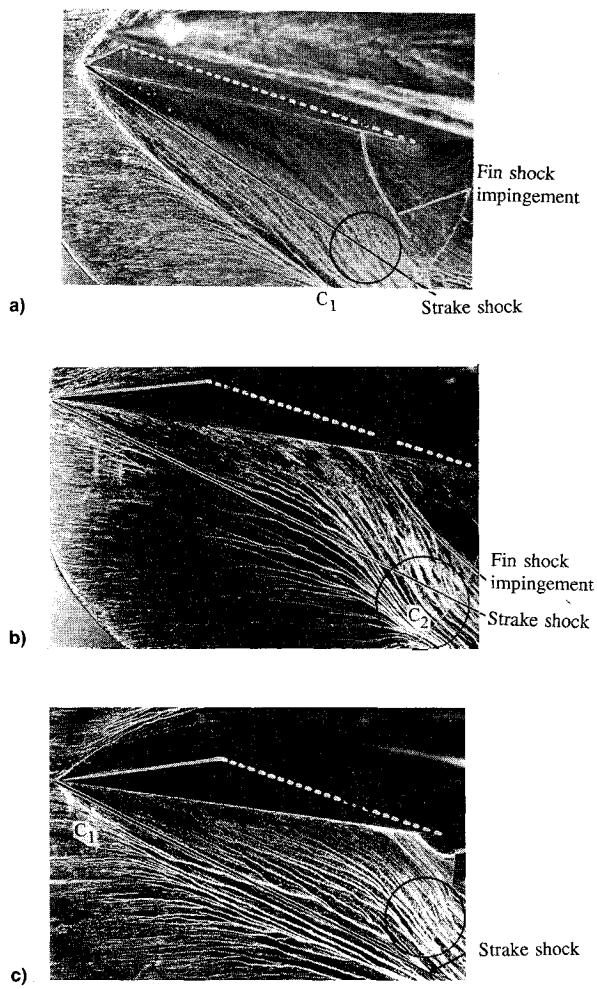

Fig. 11 Oil-flow patterns on the wall with PR_{eq}, L_{imp}/L_{fin}, and PR_{LEF}: a) strake 1 ($PR_{eq} = 1.87$, $L_{imp}/L_{fin} = 0.79$, $PR_{LEF} = 1.13$); b) strake 4 ($PR_{eq} = 1.33$, $L_{imp}/L_{fin} = 0.52$, $PR_{LEF} = 1.40$); and c) strake 5 ($PR_{eq} = 1.44$, $L_{imp}/L_{fin} = 1.34$, $PR_{LEF} = 1.38$).

still observed adjacent to the strake apex in the cases of strakes 3 and 5, even when PR_{eq} was below 1.55 (see the case of strake 5 in Fig. 11c). This may correspond to the very weak separation observed in, e.g., Ref. 10, but it is so small and weak that there is no practical importance for engineering design.

On the other hand, the oil-streak deflection caused by the fin-shock impingement becomes strong with weakening PR_{eq} (see the areas surrounded by circles in Fig. 11). The deflection was very faint in the cases of strakes 1 and 2, but led to a very vivid oil convergence observed for strakes 3 and 4 (see the convergence marked C_2 in Fig. 11b). This is because the strength of LEF is intensified by weakening PR_{eq}. Comparing the LFV images of strakes 1 and 2, the fin shock behind the strake shock was more vivid in the case of strake 2, whose strake shock was weaker than that of strake 1. From the flow past two successive wedges whose combined turning angle is fixed, it is reasonable to suppose that the fin shock behind the strake shock becomes strong with weakening of the strake shock and vice versa.

This mutual dependence can be considered quantitatively by introducing the pressure ratio across the LEF, PR_{LEF}. The value of PR_{LEF} has been read from the computed inviscid flowfields (see the example in Fig. 8) and is also printed in Fig. 11. It has been observed from all the cases examined that PR_{LEF} increases with weakening PR_{eq} and the oil deflection in the circle is enhanced with PR_{LEF}. Strake 5 has a relatively large PR_{LEF}. But no vivid oil coalescence appears (see Fig. 11c), because the fin-shock impingement point is downstream of the fin-trailing edge as L_{imp}/L_{fin} indicates.

Thus, it seems that the variables PR_{eq} and L_{imp}/L_{fin} control the actual surface oil-streak behavior. Strake 5 located in the no separation zone (see Fig. 10) could indeed prevent separation. Hence, the predicted dimensions of the strake based on these variables are also considered to be plausible. More experimental data at different flow conditions are now required in order to "validate" the prediction, which will be generalized for other fin wedge angles and flow conditions in the next section.

Effects of Various Factors on the Required Strake Dimensions

When the freestream Mach number M_∞ increases, a longer strake is necessary to reduce the strake apex angle α_{str}. Otherwise the strake-shock strength will increase with M_∞. On the other hand, the strake height required is reduced since the fin-shock propagation angle η, which depends on the Mach angle behind the strake shock, decreases as M_∞ increases (see the geometrical relation in Fig. 9).

If the fin wedge angle α_{fin} is increased, a longer strake is necessary to prevent α_{str} (and, hence, the strake-shock strength) from increasing. But the required strake height need change very little since η is independent of α_{fin}.

When the boundary-layer displacement thickness increases relative to the chord of the fin (i.e., δ^*/L_{fin} increases), the fin shock reaches the edge of the displacement thickness sooner (see Fig. 9). In order to delay the arrival, a taller strake is needed. However, the strake shock is strengthened by a strake whose sweep-angle λ decreases with strake height. Hence, a greater length is also necessary to "sharpen" the strake while maintaining the required strake height.

As already discussed, the effects of the fin wedge angle and flow conditions (α_{fin}, M_∞, and δ^*/L_{fin}) on the required strake dimensions can be considered quantitatively. In Fig. 12, the levels of the required strake height and length obtained by Eqs. (10) and (11) are plotted using a group of single-chain-dotted lines (iso-H_{req}/L_{fin} lines) and solid lines (iso-L_{req}/L_{fin} lines), respectively, over an appropriate range of M_∞ and α_{fin} for $\delta^*/L_{fin} = 0.0273$. The present experimental condition ($M_\infty = 2.46$ and $\alpha_{fin} = 15$ deg) is indicated by a solid circle in the figure. The values read from the circle, $L_{req}/L_{fin} = 0.53$ and $H_{req}/L_{fin} = 0.57$, are the same as those obtained from the point R in Fig. 10. From this chart, one can easily estimate the values of L_{req}/L_{fin} and H_{req}/L_{fin} for a wide range of M_∞ and α_{fin}.

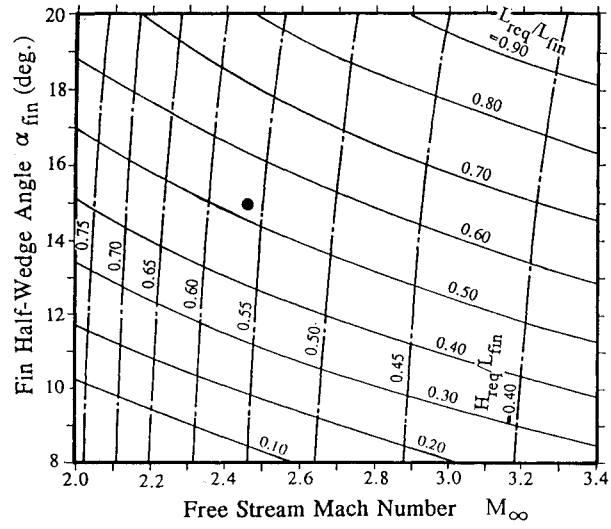

Fig. 12 Effects of M_∞ and α_{fin} on the required strake dimensions ($\delta^*/L_{fin} = 0.0273$).

The value of δ^*/L_{fin} has been fixed for Fig. 12. This factor has a relatively small role because the chord of the fin is usually much larger than δ^*. However, for an extremely thick boundary layer and (or) a relatively short fin-chord length, this factor will be more important (see Ref. 7).

Conclusions

1) A properly designated strake, which covers the whole of the root chord of a sharp fin, has a weakening effect on separation.

2) When a sharp fin is modified using a strake, a shock wave from the strake leading edge (strake shock) intersects the shock from the unmodified part of the model (fin shock) and bends it strongly toward the model. The strengths of the strake shock and the bent fin shock have strong mutual dependence.

3) The bent fin shock propagates towards the wall quite linearly with distance from the leading edge. The propagation angle is similar to the Mach angle based on the Mach number behind the strake shock.

4) In order to prevent separation, a strake must be tall enough to prevent the fin-shock reaching the wall before the fin trailing edge location. In addition, the strake must have a small apex angle and a large sweep angle so that the strake shock itself does not cause separation. Based on these conditions, the strake dimensions needed to prevent the interaction-induced separation can now be predicted. This prediction is applicable for a wide range of Mach numbers, boundary-layer displacement thicknesses, and fin wedge angles.

Acknowledgments

The present study was supported by the Technical Research & Development Institute of the Japan Defense Agency. The work reported here forms a part of the Ph.D. Dissertation of S. Koide.

References

[1]Settles, G. S., and Dolling, D. S., "Swept Shock/Boundary Layer Interactions—Tutorial and Update," AIAA Paper 90-0375, Jan. 1990.

[2]Lakshmanan, B., and Tiwari, S. N., "Study of Supersonic Intersection Flowfield at Modified Wing-Body Junctions," *AIAA Journal*, Vol. 31, No. 5, 1993, pp. 877–883.

[3]Blank, S. C., "Passive Techniques for Controlling the Flow in Supersonic Wing-Body Junctions," Ph.D. Dissertation, Cranfield Univ., Bedford, England, UK, 1994; see also Blank, S. C., "Supersonic Wing/Body Interference," International Council of the Aeronautical Sciences, ICAS-92-7.9.2, Sept. 1992.

[4]Kleifges, K., and Dolling, D. S., "Control of Unsteady Shock-Induced Turbulent Boundary Layer Separation Upstream of Blunt Fins," AIAA Paper 93-3281, July 1993.

[5]Koide, S., and Stollery, J. L., "Effects of Junction Modifications on Sharp-Fin-Induced Shock Wave/Boundary Layer Interaction," AIAA Paper 93-2935, July 1993.

[6]Kubota, H., and Stollery, J. L., "An Experimental Study of the Interaction Between a Glancing Shock Wave and a Turbulent Boundary Layer," *Journal of Fluid Mechanics*, Vol. 116, March 1982, pp. 431–458.

[7]Koide, S., "The Effects of Junction Modifications on Sharp-Fin-Induced Glancing Shock Wave/Turbulent Boundary Layer Interaction," Ph.D. Dissertation, Cranfield Univ., Bedford, England, UK, 1994.

[8]Griesel, C. J. W., "Space Marching with Rieman-Solver Adaptations Applied to Three Dimensional Flows," M.Sc. Thesis, Cranfield Inst. of Technology, Bedford, England, UK, 1993.

[9]Korkegi, R. H., "A Simple Correlation for Incipient Turbulent Boundary-Layer Separation Due to a Skewed Shock Wave," *AIAA Journal*, Vol. 11, No. 11, 1973, pp. 1578, 1579.

[10]Fomison, N. R., and Stollery, J. L., "The Effects of Sweep and Bluntness on a Glancing Shock Wave Turbulent Boundary Layer Interaction," AGARD CP 428, April 1987.